Geophysical Research Letters®

Key Points:
- Natural and simulated river meander belts reach a saturated state whereby oxbows are arranged ~1 meander radius away from each other
- Distribution of floodplain sediment age is controlled by meander location, sizes, and channel migration rate
- Natural and numerically simulated floodplains display similar relationships between their width and sediment-age distribution

Supporting Information:

Supporting Information may be found in the online version of this article.

Correspondence to:

A. Ielpi,
alessandro.ielpi@ubc.ca

Author Contributions:

Conceptualization: A. Ielpi, A. Graham
Data curation: A. Ielpi, D. P. Viero, A. Graham
Formal analysis: A. Ielpi, M. G. A. Lapôtre, A. Graham
Funding acquisition: A. Ielpi
Investigation: A. Ielpi, A. Graham, A. Finotello
Methodology: A. Ielpi, D. P. Viero, M. G. A. Lapôtre, A. Graham, A. Finotello
Project Administration: A. Ielpi
Resources: A. Ielpi
Software: A. Ielpi, D. P. Viero
Supervision: A. Ielpi
Validation: A. Ielpi, D. P. Viero, M. G. A. Lapôtre

How Is Time Distributed in a River Meander Belt?

A. Ielpi[1] [ID], D. P. Viero[2] [ID], M. G. A. Lapôtre[3], A. Graham[4] [ID], M. Ghinassi[5], and A. Finotello[5,6] [ID]

[1]Department of Earth, Environmental and Geographic Sciences, University of British Columbia-Okanagan, Kelowna, BC, Canada, [2]Department of Civil, Environmental and Architectural Engineering, University of Padua, Padua, Italy, [3]Department of Earth & Planetary Sciences, Stanford University, Stanford, CA, USA, [4]Harquail School of Earth Sciences, Laurentian University, Sudbury, ON, Canada, [5]Department of Geosciences, University of Padua, Padua, Italy, [6]Department of Environmental Sciences, Informatics, and Statistics, Ca'Foscari University of Venice, Venice, Italy

Abstract River meandering controls the age of floodplains through its characteristic paces of growth and eventual cutoff of channel bends, forming oxbows. Hence, floodplain-age distributions should reflect a river's characteristic size and migration rate. This hypothesis has been previously tested in numerical simulations, yet without systematic comparisons with natural systems. Here we analyze oxbow spacing and timescales of bend evolution and abandonment in natural and numerically simulated meander belts. In both cases, a saturated state is achieved whereby oxbows are spaced ~1 meander radius apart. At saturation, the distribution of floodplain ages and probability of sediment-storage time can be constrained from characteristic timescales of bend evolution and abandonment. Owing to the similar relationships between floodplain width and characteristic timescales in natural and simulated rivers, we postulate that this approach should apply to unconfined meandering rivers elsewhere—a hypothesis to be tested with independent geo- or dendrochronological data.

Plain Language Summary Meandering rivers have curvy channels characterized by erosion and deposition along their inner and outer banks, respectively. Over time, continued erosion and deposition shuffle sediment along the river plain, and lead to channel bends joining each other, through a process—called neck cutoff—that isolates a channel segment in between. These processes control the age of sediment and soil in a river plain over timespans much longer than human life, such that evolution models of meandering rivers often rely on numerical simulations. Here, data from both natural and simulated rivers show that, over time, neck cutoffs find themselves in closely spaced arrangements, and that their position can inform typical sediment ages once the river's characteristic pace of erosion and deposition are accounted for. These results may be tested in the future with direct age determination and, if corroborated, could further inform future studies on river organic-carbon budgets.

1. Introduction

Neck cutoff is fundamental to the planform evolution of meandering rivers, and takes place when a mature loop is isolated by the connection of its two adjacent bends. Neck cutoff completes a meander's life cycle by isolating it from the active channel (Hooke, 2013; Pannone & De Vincenzo, 2022), and maintains the river's steady state planform (Stølum, 1996). Cutoffs generate perturbations in channel slope (and thus bed stresses) as the river diverts to a shorter and steeper path, as well as in sediment supply due to neck failure (Monegaglia & Tubino, 2019; Zinger et al., 2011). The two, in turn, typically induce channel widening, faster migration, and clustering of subsequent cutoffs over scales capped by the river's backwater length (Hooke, 1995; Ielpi et al., 2021; Schwenk & Foufoula-Georgiou, 2016).

An intriguing facet of river meandering lies in the interplay between channel migration and intervening neck cutoff, which together control the age distribution of floodplain sediments (Bradley & Tucker, 2013; Howard & Knutson, 1984), with important ramifications for the study of terrestrial organic-carbon fluxes (Torres et al., 2017). The pace over which meander bends evolve from inception to neck cutoff ultimately depends on the characteristic meander size and the parent channel's migration rate. Through their relationships with the channel's hydraulic characteristics (J. A. Constantine et al., 2014; Ielpi & Lapôtre, 2020; Williams, 1986), the two are expected to impart predictable floodplain-age distribution. We test this fundamental hypothesis through a compilation of ~2,400 abandoned meanders (i.e., "oxbows") from natural rivers with global distribution and a numerical simulation of timelapse floodplain development. We show that, once a meandering river has reached a state of dynamic planform equilibrium prone to reoccurring neck cutoffs, simple metrics based on its meanders'

Visualization: A. Ielpi
Writing – original draft: A. Ielpi
Writing – review & editing: A. Ielpi, D.
P. Viero, M. G. A. Lapôtre, A. Graham,
M. Ghinassi, A. Finotello

location, size, and channel-migration rate control the floodplain-age structure. Our results bear significance to our understanding of stratigraphic time in fluvial records, and offer novel testable hypotheses for modeling carbon-age structure in floodplains.

2. Materials and Methods

Data from natural systems include the centerlines of 1,209 oxbows from the floodplains of seven freely meandering rivers with channel widths spanning ∼30–∼400 m, found in polar (Mason and Tivteyakha rivers), cold-temperate (Chinchaga and Vermilion rivers), and tropical (Juruá, Mamoré, and Mamberamo rivers) climate zones (Figures 1a–1c; Table S1 in Supporting Information S1). The banks of the actively migrating channel of the parent rivers were digitized using Landsat 7–8 and WorldView/GeoEye constellation satellite imagery and then compared over timespans of ∼20–30 years, allowing for a dynamic time warping analysis (Giorgino, 2009) of migration rates, M_r, based on the timelapse position of the channel centerlines (Text S1 in Supporting Information S1). None of the selected natural rivers show evidence for recent avulsion or branching, such that their aggradation timescales are likely orders of magnitude longer than their migration timescales (Ielpi et al., 2020; Jerolmack & Mohrig, 2007).

A numerical simulation of meandering channels capable of reaching a dynamic steady state prone to neck cutoff was conducted by modifying the *Fortran* code of the freely distributed numerical model of Bogoni et al. (2017) (see also Frascati and Lanzoni (2009)), which is coupled with the hydrodynamic and morphodynamic model of Zolezzi and Seminara (2001) (Text S2 in Supporting Information S1). Whereas lateral morphodynamics are modeled, vertical aggradation and erosion of the channel and floodplain are neglected for practical comparison with the natural rivers (owing, again, to their long aggradation over short migration timescales), and a constant floodplain slope is assumed during the simulation instead (Bogoni et al., 2017). The simulation is performed in nondimensional space, with an intrinsic distance unit equaling one channel width, w, and with the centerline migration rate calculated following the model of Ikeda et al. (1981), whereby:

$$M_r = E\,U_b, \tag{1}$$

where E and U_b are a long-term erosion coefficient and the excess near-bank velocity, respectively (Text S2 in Supporting Information S1) (Bogoni et al., 2017). Notably, E can be tuned to adjust migration rates, thereby compressing or dilating simulation time (Text S2 in Supporting Information S1). Upon developing a tight channel bend whereby neck width equates w, a neck cutoff is recorded. The simulation produced (Figures 1d–1g): (a) a final floodplain-age raster map; (b) a channel centerline at fixed time intervals; (c) a vector data set containing the oxbows lines that have survived later overprinting by the migrating channel; and (d) a matrix tallying the temporal intervals that each floodplain surface-area unit has spent between channel-reworking episodes (Text S2 in Supporting Information S1).

Morphometric data were extracted from natural and simulated floodplains using an ad-hoc algorithm written in R (Supporting Information S1), including: the Euclidean distance of an oxbow from its nearest neighbor (d_n), based on their respective neck mid-point coordinates, and from the channel's centerline (d_c) derived from the youngest imagery (for natural systems) or final planform arrangement (for simulated systems); oxbow length (l_x) and maximum radius inscribed within (r_x) (Figures 1b and 1c); the number of preserved oxbows (n_x); the total floodplain (A_f) and channel-belt (A_c) surface areas (the latter referring to the rectangular footprint of the active centerline as defined by its minimum and maximum latitudinal and longitudinal coordinates); the total centerline sinuosity index (i.e., along-channel centerline length over Euclidean distances between its extremities; χ_c); and an average bend sinuosity index, integrating data from all the individual bends in the active centerline ($\overline{\chi}_b$) identified based on local curvature maxima (Schwenk & Foufoula-Georgiou, 2016).

The number of oxbows per surface area is used as a proxy for the spatial density of oxbows in the floodplain ($\rho_x = n_x/A_f$). Other extracted information related to temporal trends of floodplain evolution includes the final age of individual floodplain parcels at the end of the simulation (T_f), the storage time of sediment between successive reworking episodes for all floodplain parcels that underwent overprinting at least once (T_s), and actual oxbow age (T_x). The simulation presented here encompasses 500 kyr, with outputs produced at 1 kyr intervals (Figures 2a–2f; Table S2 in Supporting Information S1). The first 10 kyr in the numerical simulation are not recorded, as this time interval witnesses the initial evolution of the channel centerline from straight to sinuous and cutoff-prone.
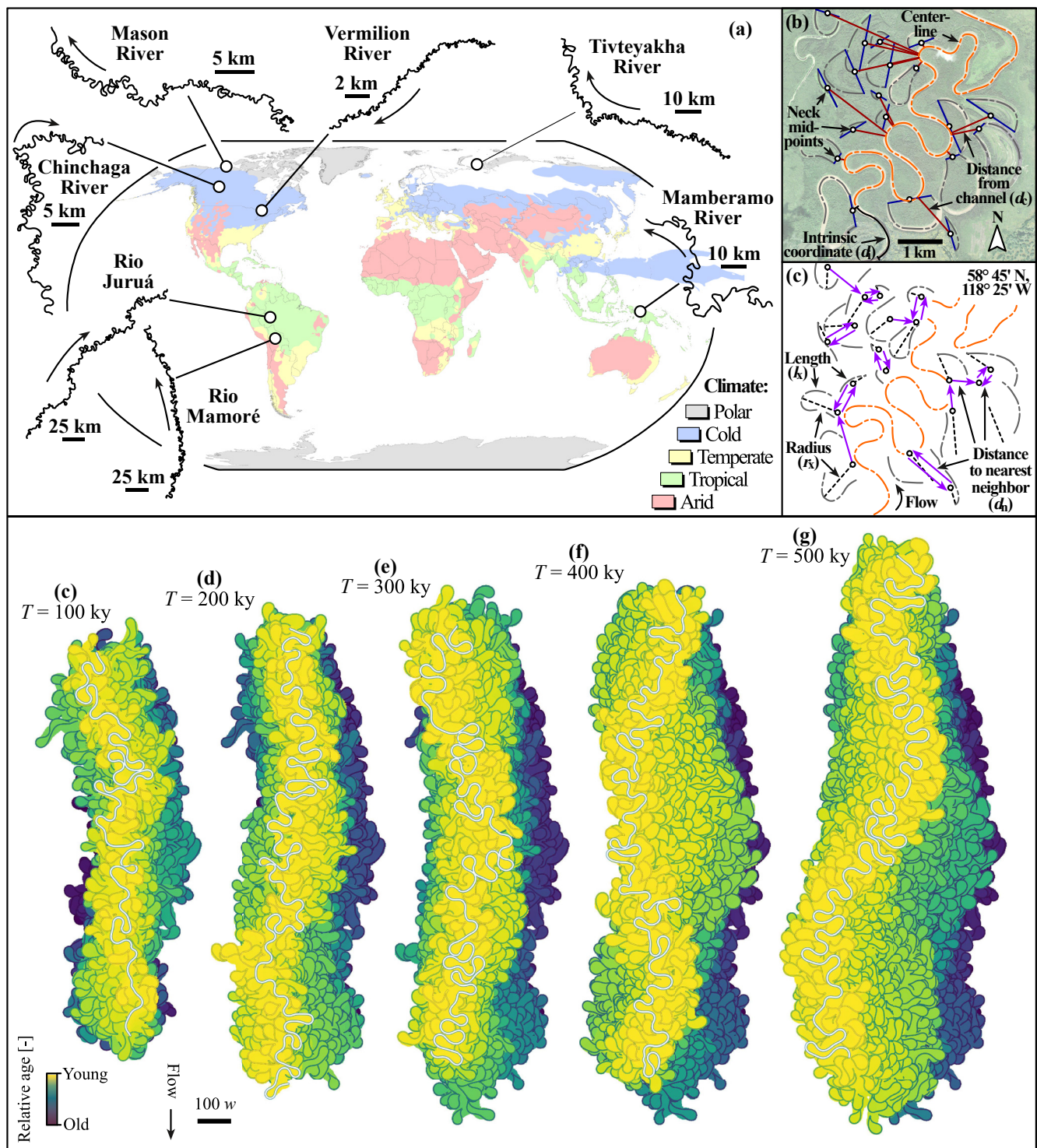
Figure 1. Data set. (a) Selected natural rivers, with climate zones from Beck et al. (2018) reported. Centerlines of the Juruá and Mamoré rivers are from Sylvester et al. (2019). (b, c) Satellite view of a reach of the Chinchaga River (Alberta, Canada), with illustrations of the main extracted morphometric parameters. See "Section 2" for details. (d–g) Maps of numerical simulation outputs at 100 kyr intervals, including relative ages of floodplain and oxbows, and channel centerline.
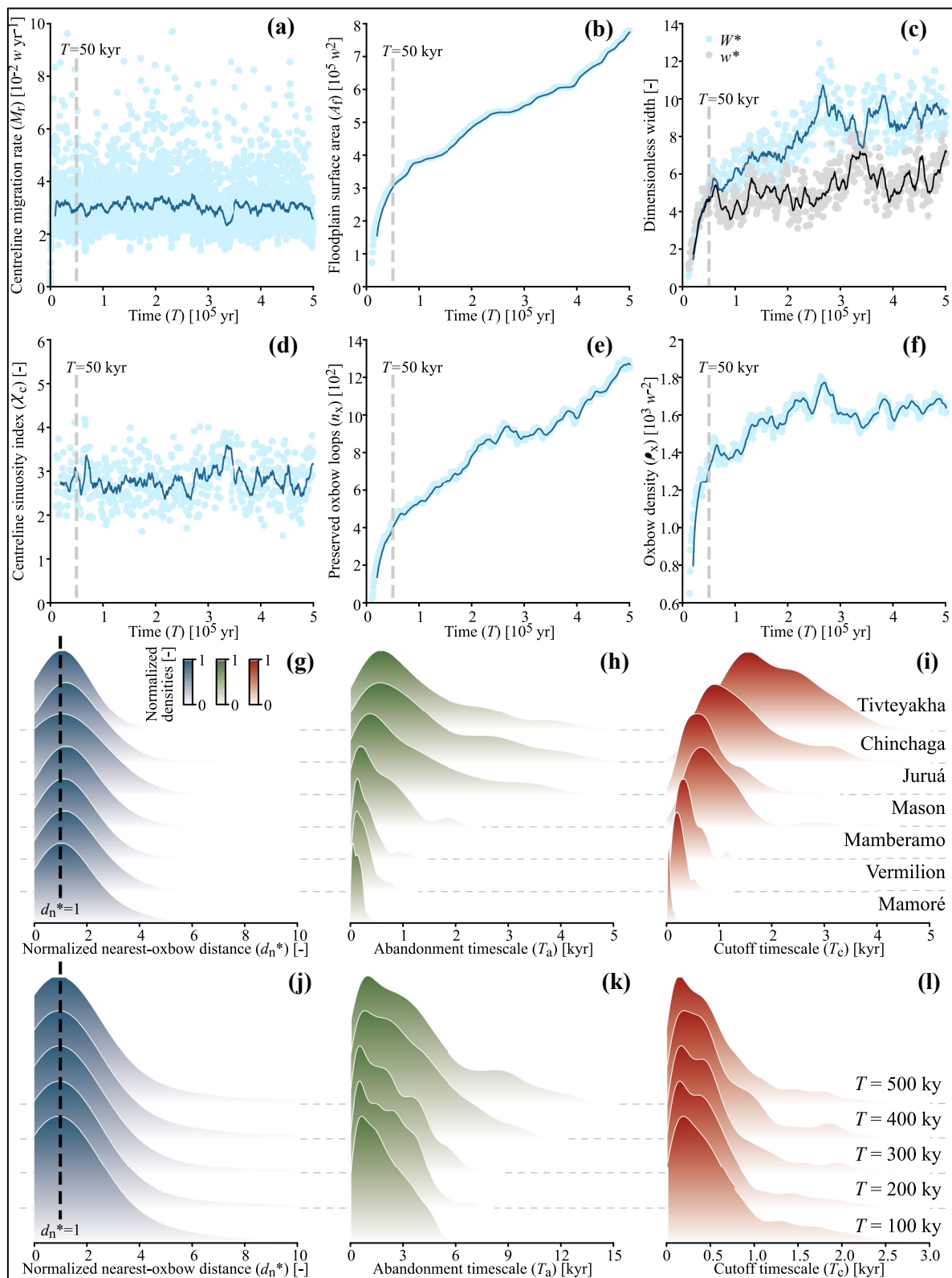
Figure 2.

2.1. Dimensionless Metrics

To explore the spatial distribution of oxbows in a meander belt, a normalized nearest-oxbow distance is defined as

$$d_n^* = d_n / \bar{r}_x, \tag{2}$$

a metric that describes the distance between neck mid-points in units of mean oxbow radius ($\bar{r}_x$). Then, to explore the frequency of cutoff events and related floodplain-age structure, an abandonment timescale is defined as

$$T_a = d_c / M_r, \tag{3}$$

that is, a lower bound of oxbow age in a simplified scenario where the channel migrated away from cutoff bends orthogonally, and without reversals, at a constant rate M_r. Similarly, a cutoff timescale is defined as

$$T_c = r_x / M_r, \tag{4}$$

which approximates the time taken by a meander to grow to the point of neck cutoff assuming a steady M_r. Whereas M_r is complexly modulated by curvature (Schwenk et al., 2015; Sylvester et al., 2019), it tends to plateau along sharper bends (Finotello et al., 2019), such that the assumption of steady M_r in growing meanders is preferred here for simplicity. Dimensionless floodplain (W^*) and channel-belt (w^*) widths are respectively defined as

$$W^* = \frac{A_f}{l_c \, r_{x,50}}, \text{ and} \tag{5a}$$

$$w^* = \frac{A_c}{l_c \, r_{x,50}}. \tag{5b}$$

where l_c is the length of the active centerline. The two metrics provide a proxy for the width of the floodplain and channel belt (which scale, respectively, with A_f/l_c and A_c/l_c) in units of median meander radii ($r_{x,50}$). Finally, to facilitate the comparison of abandonment timescales and sediment-storage durations between natural and simulated floodplains, we normalize T_a and T_s by the modal value of cutoff timescale, $T_{c,mod}$ (Torres et al., 2017), as follows:

$$T_a^* = T_a / T_{c,mod}, \text{ and} \tag{6a}$$

$$T_s^* = T_s / T_{c,mod}. \tag{6b}$$

3. Results

3.1. Numerical Simulation

A roughly constant $M_r/w \cong 0.03$ is maintained throughout the simulation with $E = 10^{-9}$ (Figure 2a); this migration pace is broadly comparable to that of the natural rivers considered here (Table S1 in Supporting Information S1) and of pristine vegetated meanders elsewhere (J. A. Constantine et al., 2014; Finotello et al., 2019; Ielpi & Lapôtre, 2020; Sylvester et al., 2019). The total floodplain surface area, A_f, grows logarithmically through time in the first 50 kyr and then roughly linearly over the following 450 kyr (Figure 2b). The dimensionless floodplain and channel-belt widths, W^* and w^*, grow through time following similar trends until 50 kyr, and diverge later on (Figure 2c). The total centerline sinuosity index, χ_c, remains roughly constant at ~2–4 throughout the simulation (Figure 2d). Notably, the average bend sinuosity index, $\overline{\chi}_b$, plateaus at ~1.5–2.0 within the first 10 kyr of the simulation, and remains stable afterward (Table S2 in Supporting Information S1). The number of preserved oxbows, n_x (Figure 2e) and spatial density of oxbows in the floodplain, ρ_x (Figure 2f) also grow

Figure 2. Results. (a–f) Evolution of the simulated floodplain. Displayed as a function of time are (a) migration rate, (b) total floodplain surface area, (c) dimensionless floodplain and channel belt widths, (d) total centerline sinuosity index, (e) number of preserved oxbows, and (f) oxbow density. Solid lines report 10-point moving averages. A number of parameters stabilize or grow (near-)linearly since 50 kyr. (g–l) Kernel Density Estimation plots showing the distribution of normalized nearest-oxbow distance ((g and j) for, respectively, natural and simulated oxbows), abandonment timescale ((h and k) for, respectively, natural and simulated oxbows), and cutoff timescale ((i and l) for, respectively, natural and simulated oxbows). Natural rivers are arranged based on timescale distribution-tail lengths.
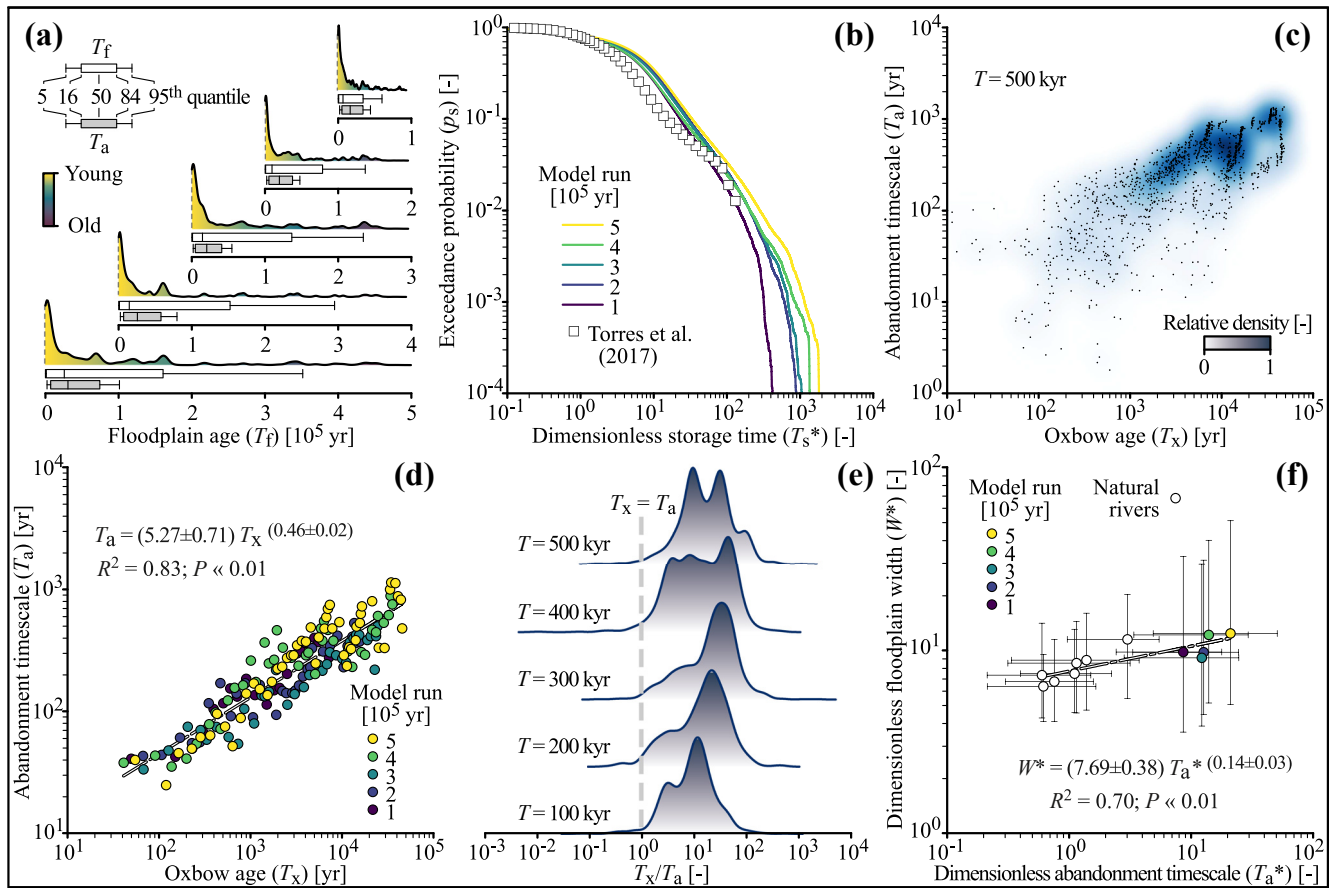
Figure 3. Distribution of time metrics in the numerical simulation, and comparison with natural rivers. *P*-values for regressions refer to the *F*-test of overall significance. (a) Kernel Density Estimation (KDE) plots, color-coded by relative age, of simulated floodplain age, with box plots reporting its summary statistics against those of abandonment timescale. (b) Exceedance probability of dimensionless sediment storage time in the simulation, with data from Torres et al. (2017) reported. (c) Simulated abandonment timescale as a function of actual age for the final simulation state. The bivariate KDE map shows how most preserved oxbows attain actual age of $\sim 10^3$–10^5 and an abandonment timescale of $\sim 10^2$–10^3 yr. (d) Data binning (25-point mean) of oxbow actual versus abandonment timescale, showing a strong and statistically significant power-law relationship between the two metrics in the simulation. (e) KDE plots of the ratio between the actual age of oxbows and abandonment timescale in the simulation, showing the departure between the two metrics. (f) Dimensionless abandonment timescale plotted as a function of dimensionless floodplain width.

logarithmically through time in the first 50 kyr and then follow a roughly linear trend, though with significant oscillations.

3.2. Spatial and Temporal Oxbow Distributions

Normalized nearest-oxbow distance, abandonment timescale, and cutoff timescale all show positively skewed distributions in both natural and simulated oxbows (Figure 2g–2l, Figure S2, and Table S2 in Supporting Information S1). Distributions of normalized near-oxbow distance, d_n^*, show very little variation across natural and simulated oxbows (Figures 2g and 2j), with a pronounced mode at ~ 1 (indicating that most oxbows are located about 1 meander radius away from each other). The abandonment timescale, T_a, shows variable distributions in natural rivers, with modes from individual rivers at ~ 50–~ 600 years (Figure 2h) and long tails for the Chinchaga, Juruá, and Tivteyakha rivers. The abandonment timescale of simulated oxbows attains less dispersed modes at ~ 500–$1,000$ years; these modes slightly increase over longer simulation timespans, a trend that is accompanied by a likewise increasingly positive skew in the distributions (Figure 2k). The cutoff timescale, T_c, attains dispersed values in natural oxbows, with modes of individual rivers ranging from ~ 40 to $\sim 1,500$ years and likewise longer tails for the Chinchaga, Juruá, and Tivteyakha rivers (Figure 2i). Simulated oxbows attain overall consistent distributions of cutoff timescale, with main modes at ~ 150–200 years, and a secondary, poorly defined mode at $\sim 2,000$ years (Figure 2l).

The analysis of floodplain age, T_f, reveals a strong skew toward younger ages (Figure 3a), indicating how preservation of old floodplain swaths becomes less likely with time (Huffman et al., 2022). Dimensionless storage time, T_s^*, is assessed against its exceedance probability, p_s (Figure 3b), which decreases through a complex pattern defined by a shallowly sloping power-law trend at $T_s^* < 10$, an essentially linear trend at $T_s^* \sim 10$–200, and a steeply sloping power-law trend at $T_s^* > 200$. Considering the full simulation, the best-fitting power-law exponents for the three trends are, respectively, −0.27, −1.03, and −2.17. We find a ∼92% and ∼97% probability that any point in the floodplain is younger than 1 and 10 cutoff timescales, respectively (Figure 3b).

Finally, abandonment timescales and actual simulated ages are compared. At the end of the simulation, most preserved oxbows have actual ages, T_x, of 10^3–10^5 yr, yet they record abandonment timescales, T_a, of 10^2–10^3 yr (Figure 3c). Despite data scattering, data binning in the {T_x; T_a} space reveals a strong and statistically significant power-law relationship between the two metrics (Figure 3d). The ratio between the two ages (T_x/T_a) likewise shows that, throughout the simulation, T_a overall underestimates T_x by ∼1–2 orders of magnitude (Figure 3e).

4. Discussion and Conclusions

The numerical simulation conducted here reveals two initial characteristic timescales related to the achievement of dynamically stable planform dynamics. Over the first 10 kyr, the channel centerline evolves from linear to sinuous and cutoff-prone. Then, until 50 kyr, the simulation is characterized by a floodplain that approximates in width the spatial domain occupied by the active centerline (Figure 2c). In such a state, outward migration of the centerline is likely to impart growth on both sides of the floodplain, thereby contributing to its fast expansion (Figures 2b and 2c). Beyond 50 kyr, the floodplain has become wide enough such that it is likely to grow on one hydrographic side at a time only, rather than along both contemporaneously. We interpret this morphodynamic transition as the cause of stepwise transitions in floodplain-growth rate (Figures 2b and 2c) and related oxbow preservation (Figures 2e and 2f).

Regardless of its growth rate, the simulated floodplain's record of long-term stationarity in channel migration rate and sinuosity (Figures 2a and 2d) suggests that morphodynamic comparisons can be explored between the latter and natural floodplains. This hypothesis is corroborated by the record of similar distributions of normalized nearest-oxbow distance, d_n^*, and specifically of matching modes at ∼1 meander radius (Figures 2g and 2j). We interpret the matching peaks as an indication that both natural and simulated floodplains have reached what we define as *oxbow saturation*, that is, a saturated state whereby any newly emplaced oxbow will most likely overprint previous ones, such that no tighter planform re-arrangement at average distances shorter than ∼1 characteristic meander radius can be attained in the long term. Saturation is further highlighted by plateauing oxbow density beyond 50 kyr (Figure 2f), indicating that juvenile floodplains that have not reached saturation yet will be characterized by fewer and farther-apart oxbows with $d_n^* \gg 1$. Normalized nearest-oxbow distance could therefore be analyzed in natural floodplains that have undergone recent planform adjustments in response to autogenic processes or external stressors (Greenberg & Ganti, 2021; Horn et al., 2012; Monegaglia & Tubino, 2019; Schwenk & Foufoula-Georgiou, 2016), to test whether a new state of equilibrium was reached.

Remarkably, the mode at $d_n^* \sim 1$ is present in both natural and simulated floodplains despite strikingly diverse distributions of abandonment and cutoff timescales (Figures 2g and 2j), suggesting that oxbow saturation is a geometric phenomenon related to the optimization of space filling (Dodds & Rothman, 2000; Edmonds et al., 2011), and independent of the river's characteristic size and migration rate. The latter two parameters, instead, control the diverse distributions of abandonment and cutoff timescales in natural rivers: differences in their distributions (Figures 2h and 2i) inform the geomorphic variability arising from the interplay between lateral-migration rates and the alluvial plain's characteristic sizes (e.g., lateral floodplain width, which ultimately controls the distances of oxbows from an active channel, and meander size) (J. A. Constantine et al., 2014; Leopold et al., 1964; Williams, 1986). Specifically, natural rivers will attain higher kurtosis and lighter tails in their distributions of abandonment and cutoff timescales when smaller meander belts migrate at a comparatively fast rate (e.g., Mamoré), and vice versa (e.g., Tivteyakha) (Figures 2h and 2i). As migration rate scales with bank erodibility (Equation 1), we note that the broader range in abandonment and cutoff timescales for natural floodplains over simulated ones likely reflects natural variability in bank strength (C. R. Constantine et al., 2009), which is instead constant and homogenous in the numerical simulation. Finally, since the abandonment-timescale distributions of simulated oxbows attain longer tails with time (Figure 2k), we theorize that the different distributions of the same timescale in natural rivers likewise could arise from different durations of meander-belt

evolution (e.g., different times since the inception of meandering or, in sharply aggradational systems elsewhere, since the last avulsion event).

Our simulation shows how, through channel migration, bend evolution, and meander cutoff efficiently rejuvenate older floodplain swaths; the timeseries of floodplain-age distribution presented in Figure 3a show a *push-broom* style of floodplain rejuvenation whereby the floodplain-age mode is remarkably small, and independent of the simulation time. Notably, the $\pm 2\sigma$ range around the mode of the abandonment timescale captures roughly 2/3 of the distribution of floodplain ages (Figure 3a), and its 5th quantile is an accurate predictor of the modal floodplain age (with relative errors of 1.2%–3.6%). We therefore posit that, in likewise unconfined natural meandering-river floodplains that have reached oxbow saturation, the abandonment timescale may be used as a simple yet useful proxy to inform floodplain-age distribution.

The arguments presented above also apply to the predictive analysis of sediment-storage times in a floodplain. As older floodplain swaths are less commonly preserved than younger ones, the distribution of dimensionless storage time, T_s^*, is likewise skewed toward short intervals (Figure 3b) (Bradley & Tucker, 2013). We observe an increase in the largest T_s^* recorded with longer simulation runs (Figure 3b), as expected in a scenario where the oldest possible storage time increases with meander-belt age. Differences between the individual distributions, however, become significant only for $T_s^* > 10$, that is, in a scenario with exceedance probability (p_s) $<\sim 3\%$ even in simulated floodplains that are free to grow laterally without any constriction for 500 kyr. Our results accordingly suggest that a simple estimate of the cutoff timescale, through inversion, can be used to inform actual storage times (Figure 3b). The distribution of dimensionless sediment storage times broadly compares to what obtained by Torres et al. (2017), yet with a departure that is most pronounced at $T_s^* \approx 10$ (Figure 3b), for which a difference in p_s of <0.2 is observed. Assuming otherwise comparable numerical setups, the departure in probability distribution can be related to differences in the normalization parameter, T_c, which, in Torres et al. (2017), is calculated using an explicit tracking method (Schwenk et al., 2015) instead of our simpler metric of oxbow radius over migration rate (Equation 4).

The abandonment timescale, as expected, underestimates the actual oxbow age, although it does so in a predictable fashion. Specifically, albeit data scattering (Figures 3c and 3e), binning shows a strong relationship between the two age metrics (Figure 3d). This consideration discloses two important aspects: (a) departures between actual age and abandonment timescale of natural oxbows can be investigated through geochronology (e.g., ^{14}C) (Ishii & Hori, 2016; Wren et al., 2008) or dendrochronology (Malik, 2006; Nakamura, 1986) in future studies, allowing further tests between natural and simulated meander belts; and (b) the distribution of ratios between oxbow age and abandonment timescale (Figure 3e) depicts how much information is lost in a floodplain through reworking. Despite aggradation is not modeled herein, the latter aspect may warrant forthcoming comparisons with other metrics of stratigraphic completeness in both recent and ancient meander belts (Durkin et al., 2018; Sadler, 1981). Whereas natural and simulated floodplains appear to observe similar relationships between dimensionless abandonment timescale and their dimensionless width (Figure 3f), simulated floodplains produced herein display limited variability in these two parameters. As such, the relationships between floodplain size and characteristic abandonment timescale may need further investigation.

Lateral confinement by, for example, terraces or valley flanks has a demonstrated control on meander morphodynamics—for example, on their capacity to migrate downstream rather than expand laterally (Ghinassi et al., 2016; Ielpi & Ghinassi, 2014), which affects their capacity to develop neck cutoffs (Nicoll & Hickin, 2010) and can shorten characteristic sediment-storage timescales (Bradley & Tucker, 2013), as recently demonstrated in the confined Powder River of Montana (Huffman et al., 2022). Since negative topography sided by terraces can be autogenically generated in meander belts without external perturbations (Lewin & Ashworth, 2014; Limaye & Lamb, 2016), our results might broadly apply to slightly incised meanders. Refined numerical simulations able to model variable degrees of channel and floodplain confinement are however necessary to test this hypothesis. That being said, our results suggest that—in both natural and simulated systems—meander belts evolve toward a state of oxbow saturation whereby oxbows are spaced ~1 meander radius apart. At saturation, simple metrics that include oxbow location, size, and the parent channel's migration rate inform characteristic timescales of bend evolution (cutoff) and abandonment. These timescales, in turn, can be used as simple yet accurate proxies for the distributions of ages in a floodplain and the probability of sediment-storage time therein.

Data Availability Statement

Analyzed data are included as Supporting Information S1, or are available in Sylvester et al. (2019). Codes and outputs employed herein are original or modified from the numerical models available in Bogoni et al. (2017), Frascati and Lanzoni (2009), and Zolezzi and Seminara (2001), and available at https://doi.org/10.5281/zenodo.7419761.

References

Beck, H. E., Zimmermann, N. E., McVicar, T. R., Vergopolan, N., Berg, A., & Wood, E. F. (2018). Present and future Köppen-Geiger climate classification maps at 1-km resolution. *Scientific Data*, *5*(1), 180214. https://doi.org/10.1038/sdata.2018.214

Bogoni, M., Putti, M., & Lanzoni, S. (2017). Modeling meander morphodynamics over self-formed heterogeneous floodplains. *Water Resources Research*, *53*(6), 5137–5157. https://doi.org/10.1002/2017WR020726

Bradley, D. N., & Tucker, G. E. (2013). The storage time, age, and erosion hazard of laterally accreted sediment on the floodplain of a simulated meandering river. *Journal of Geophysical Research: Earth Surface*, *118*(3), 1308–1319. https://doi.org/10.1002/jgrf.20083

Constantine, C. R., Dunne, T., & Hanson, G. J. (2009). Examining the physical meaning of the bank erosion coefficient used in meander migration modeling. *Geomorphology*, *106*(3–4), 242–252. https://doi.org/10.1016/j.geomorph.2008.11.002

Constantine, J. A., Dunne, T., Ahmed, J., Legleiter, C., & Lazarus, E. D. (2014). Sediment supply as a driver of river meandering and floodplain evolution in the Amazon Basin. *Nature Geoscience*, *7*(12), 899–903. https://doi.org/10.1038/ngeo2282

Dodds, P. S., & Rothman, D. H. (2000). Scaling, universality, and geomorphology. *Annual Review of Earth and Planetary Sciences*, *28*(1), 571–610. https://doi.org/10.1146/annurev.earth.28.1.571

Durkin, P. R., Hubbard, S. M., Holbrook, J., & Boyd, R. (2018). Evolution of fluvial meander-belt deposits and implications for the completeness of the stratigraphic record. *Bulletin of the Geological Society of America*, *130*(5–6), 721–739. https://doi.org/10.1130/B31699.1

Edmonds, D. A., Paola, C., Hoyal, D. C. J. D., & Sheets, B. A. (2011). Quantitative metrics that describe river deltas and their channel networks. *Journal of Geophysical Research*, *116*(4), F04022. https://doi.org/10.1029/2010JF001955

Finotello, A., D'Alpaos, A., Lazarus, E. D., & Lanzoni, S. (2019). High curvatures drive river meandering: COMMENT. *Geology*, *47*(10), e485. https://doi.org/10.1130/G46761C.1

Frascati, A., & Lanzoni, S. (2009). Morphodynamic regime and long-term evolution of meandering rivers. *Journal of Geophysical Research*, *114*(2), 1–12. https://doi.org/10.1029/2008JF001101

Ghinassi, M., Ielpi, A., Aldinucci, M., & Fustic, M. (2016). Downstream-migrating fluvial point bars in the rock record. *Sedimentary Geology*, *334*, 66–96. https://doi.org/10.1016/j.sedgeo.2016.01.005

Giorgino, T. (2009). Computing and visualizing dynamic time warping alignments in R: The dtw package. *Journal of Statistical Software*, *31*(7), 1–24. https://doi.org/10.18637/jss.v031.i07

Greenberg, E., & Ganti, V. (2021). Fluvial sediment supply controls reach-scale migration rates for meandering rivers globally. In *AGU fall meeting proceedings* (p. EP34A-06).

Hooke, J. M. (1995). River channel adjustment to meander cutoffs on the River Bollin and River Dane, northwest England. *Geomorphology*, *14*(3), 235–253. https://doi.org/10.1016/0169-555X(95)00110-Q

Hooke, J. M. (2013). River meandering. In *Treatise on geomorphology* (Vol. 9). Elsevier Ltd. https://doi.org/10.1016/B978-0-12-374739-6.00241-4

Horn, J. D., Joeckel, R. M., & Fielding, C. R. (2012). Progressive abandonment and planform changes of the central Platte River in Nebraska, central USA, over historical timeframes. *Geomorphology*, *139–140*, 372–383. https://doi.org/10.1016/j.geomorph.2011.11.003

Howard, A. D., & Knutson, T. R. (1984). Sufficient conditions for river meandering: A simulation approach. *Water Resources Research*, *20*(11), 1659–1667. https://doi.org/10.1029/WR020i011p01659

Huffman, M. E., Pizzuto, J. E., Trampush, S. M., Moody, J. A., Schook, D. M., Gray, H. J., & Mahan, S. A. (2022). Floodplain sediment storage timescales of the laterally confined meandering Powder River, USA. *Journal of Geophysical Research: Earth Surface*, *127*, 1–21. https://doi.org/10.1029/2021jf006313

Ielpi, A., & Ghinassi, M. (2014). Planform architecture, stratigraphic signature and morphodynamics of an exhumed Jurassic meander plain (Scalby Formation, Yorkshire, UK). *Sedimentology*, *61*(7), 1923–1960. https://doi.org/10.1111/sed.12122

Ielpi, A., & Lapôtre, M. G. A. (2020). A tenfold slowdown in river meander migration driven by plant life. *Nature Geoscience*, *13*(1), 82–86. https://doi.org/10.1038/s41561-019-0491-7

Ielpi, A., Lapôtre, M. G. A., Finotello, A., & Ghinassi, M. (2021). Planform-asymmetry and backwater effects on river-cutoff kinematics and clustering. *Earth Surface Processes and Landforms*, *46*(2), 357–370. https://doi.org/10.1002/esp.5029

Ielpi, A., Lapôtre, M. G. A., Finotello, A., Ghinassi, M., & D'Alpaos, A. (2020). Channel mobility drives a diverse stratigraphic architecture in the dryland Mojave River (California, USA). *Earth Surface Processes and Landforms*, *45*(8), 1717–1731. https://doi.org/10.1002/esp.4841

Ikeda, S., Parker, G., & Sawai, K. (1981). Bend theory of river meanders. Part 1. Linear development. *Journal of Fluid Mechanics*, *112*(-1), 363–377. https://doi.org/10.1017/S0022112081000451

Ishii, Y., & Hori, K. (2016). Formation and infilling of oxbow lakes in the Ishikari lowland, northern Japan. *Quaternary International*, *397*, 136–146. https://doi.org/10.1016/j.quaint.2015.06.016

Jerolmack, D. J., & Mohrig, D. (2007). Conditions for branching in depositional rives. *Geology*, *35*(5), 463–466. https://doi.org/10.1130/G23308A.1

Leopold, L. B., Wolman, M. G., & Miller, J. P. (1964). *Fluvial processes in geomorphology*. Dover Publications, Inc.. Retrieved from http://pubs.er.usgs.gov/publication/70185663

Lewin, J., & Ashworth, P. J. (2014). The negative relief of large river floodplains. *Earth-Science Reviews*, *129*, 1–23. https://doi.org/10.1016/j.earscirev.2013.10.014

Limaye, A. B. S., & Lamb, M. P. (2016). Numerical model predictions of autogenic fluvial terraces and comparison to climate change expectations. *Journal of Geophysical Research: Earth Surface*, *121*(3), 512–544. https://doi.org/10.1002/2014JF003392

Malik, I. (2006). Contribution to understanding the historical evolution of meandering rivers using dendrochronological methods: Example of the Mała Panew River in southern Poland. *Earth Surface Processes and Landforms*, *31*(10), 1227–1245. https://doi.org/10.1002/esp.1331

Monegaglia, F., & Tubino, M. (2019). The hydraulic geometry of evolving meandering rivers. *Journal of Geophysical Research: Earth Surface*, *124*(11), 2723–2748. https://doi.org/10.1029/2019JF005309

Nakamura, F. (1986). Analysis of storage and transport processes based on age distribution of sediment. *Transactions of Japanese Geomorphological Union*, *7*, 165–184.

Nicoll, T. J., & Hickin, E. J. (2010). Planform geometry and channel migration of confined meandering rivers on the Canadian prairies. *Geomorphology*, *116*(1–2), 37–47. https://doi.org/10.1016/j.geomorph.2009.10.005

Pannone, M., & De Vincenzo, A. (2022). On the prediction of the characteristic times of river meander cutoff sequence: Theoretical model and comparison with laboratory and field observations. *Water Resources Research*, *58*(7), e2021WR031661. https://doi.org/10.1029/2021WR031661

Sadler, P. M. (1981). Sediment accumulation rates and the completeness of stratigraphic sections. *The Journal of Geology*, *89*(5), 569–584. https://doi.org/10.1086/628623

Schwenk, J., & Foufoula-Georgiou, E. (2016). Meander cutoffs nonlocally accelerate upstream and downstream migration and channel widening. *Geophysical Research Letters*, *43*(24), 12437–12445. https://doi.org/10.1002/2016GL071670

Schwenk, J., Lanzoni, S., & Foufoula-Georgiou, E. (2015). The life of a meander bend: Connecting shape and dynamics via analysis of a numerical model. *Journal of Geophysical Research: Earth Surface*, *120*(4), 690–710. https://doi.org/10.1002/2014JF003252

Stølum, H. H. (1996). River meandering as a self-organization process. *Science*, *271*(5256), 1710–1713. https://doi.org/10.1126/science.271.5256.1710

Sylvester, Z., Durkin, P., & Covault, J. A. (2019). High curvatures drive river meandering. *Geology*, *47*(3), 263–266. https://doi.org/10.1130/G45608.1

Torres, M. A., Limaye, A. B., Ganti, V., Lamb, M. P., Joshua West, A., & Fischer, W. W. (2017). Model predictions of long-lived storage of organic carbon in river deposits. *Earth Surface Dynamics*, *5*(4), 711–730. https://doi.org/10.5194/esurf-5-711-2017

Williams, G. P. (1986). River meanders and channel size. *Journal of Hydrology*, *88*(1–2), 147–164. https://doi.org/10.1016/0022-1694(86)90202-7

Wren, D. G., Davidson, G. R., Walker, W. G., & Galicki, S. J. (2008). The evolution of an oxbow lake in the Mississippi alluvial floodplain. *Journal of Soil and Water Conservation*, *63*(3), 129–135. https://doi.org/10.2489/63.3.129

Zinger, J. A., Rhoads, B. L., & Best, J. L. (2011). Extreme sediment pulses generated by bend cutoffs along a large meandering river. *Nature Geoscience*, *4*(10), 675–678. https://doi.org/10.1038/ngeo1260

Zolezzi, G., & Seminara, G. (2001). Downstream and upstream influence in river meandering. Part 1. General theory and application to overdeepening. *Journal of Fluid Mechanics*, *438*, 183–211. https://doi.org/10.1017/S002211200100427X

References From the Supporting Information

Farr, T. G., Rosen, P. A., Caro, E., Crippen, R., Duren, R., Hensley, S., et al. (2007). The shuttle radar topography mission. *Reviews of Geophysics*, *45*(2), RG2004. https://doi.org/10.1029/2005rg000183

Richards, D., & Konsoer, K. (2020). Morphologic adjustments of actively evolving highly curved neck cutoffs. *Earth Surface Processes and Landforms*, *45*(4), 1067–1081. https://doi.org/10.1002/esp.4763